processes

MDPI

Article

Optimising Spread-Layer Quality in Powder Additive Manufacturing: Assessing Packing Fraction and Segregation Tendency

Hamid Salehi [1,2,*], John Cummins [2], Enrico Gallino [3], Vivek Garg [2], Tong Deng [2], Ali Hassanpour [4] and Mike Bradley [2]

[1] School of Engineering, University of Greenwich, Chatham ME4 4TB, UK
[2] Wolfson Centre, University of Greenwich, Chatham ME4 4TB, UK; john@innovationpartners.co.uk (J.C.); v.garg@gre.ac.uk (V.G.); t.deng@gre.ac.uk (T.D.); m.s.a.bradley@greenwich.ac.uk (M.B.)
[3] RICOH UK Products Ltd., Telford TF2 9N, UK; enrico.gallino@ricoh-rpl.com
[4] School of Chemical and Process Engineering, University of Leeds, Leeds LS2 9JT, UK; a.hassanpour@leeds.ac.uk
* Correspondence: hs2602e@gre.ac.uk

Abstract: Powder bed fusion (PBF), a subset of additive manufacturing methods, is well known for its promise in the production of fully functional artefacts with high densities. The quality of the powder bed, commonly referred to as powder spreading, is a crucial determinant of the final quality of the produced artefact in the PBF process. Therefore, it is critical that we examine the factors that impact the powder spreading, notably the powder bed quality. This study utilised a newly developed testing apparatus, designed specifically for examining the quality of powder beds. The objective was to analyse the influence of various factors, including the recoater shape, recoater gap size, and the different powder flow properties, on the powder bed relative packing fraction. Additionally, the study aimed to assess the variation in the particle size and shape across the build plate. The results indicated that all of the variables examined had an impact on the relative packing fraction, as well as the size and shape variations observed across the build plate.

Keywords: additive manufacturing; size and shape segregation; packing fraction; powder spreading

Citation: Salehi, H.; Cummins, J.; Gallino, E.; Garg, V.; Deng, T.; Hassanpour, A.; Bradley, M. Optimising Spread-Layer Quality in Powder Additive Manufacturing: Assessing Packing Fraction and Segregation Tendency. *Processes* **2023**, *11*, 2276. https://doi.org/10.3390/pr11082276

Academic Editor: Antonino Recca

Received: 6 July 2023
Revised: 19 July 2023
Accepted: 25 July 2023
Published: 28 July 2023

1. Introduction

Powders are critical to over 50% of the UK manufacturing output, covering both large, established industries with a strong future in the UK, subject to competitiveness, and emerging manufacturing processes [1]. Powder bed fusion (PBF) procedures are a subset of additive manufacturing and 3D printing (AM3DP) processes, in which powders are melted or sintered in the manufacturing of 3D items. In general, all PBF processes adopt a similar approach to their process chain of activities, with slight variances compensating for characteristics such as the type of energy source used, and the type of material [2].

A controlled laser or electron beam is commonly used in additive layer manufacturing (ALM) to sinter and/or melt the powders spread across the build plate; alternatively, a binder may be jetted into the layer, to bond the particles together. Multiple processes are involved in the method, which include the spreading of a layer of particles on the powder bed, and then raster scanning using a laser, electron beam, or binder jet, to sinter specific parts of the bed. This method produces a component encased in loose powder, which is then removed and recycled. The quality of the powder bed in the AM process is one of the most important aspects in determining the finished artefact's quality [2]. As a result, various investigations into quantifying the spread powder bed quality, i.e., the powder bed density (often expressed as a relative packing fraction), have been conducted. The density of a powder bed is determined by a number of elements, including the particle size

and distribution, aspect ratio, powder flowability, spreader type, and spreader velocity [2]. The majority of the results/studies listed below were derived using the DEM, without any experimental validations. In comparison to the real system, both the physical models of the particle structure, and the contact models utilised in the DEM are substantially simplified [3]. These rely on smooth spherical/cylindrical particles all of the same size, and/or a bimodal particle size distribution in a structured packing, whereas the real system has particles with sizes ranging across at least 2:1, each particle a different shape, all angular, and packed together in an almost infinite variety of juxtapositions [3].

Numerous researchers have conducted investigations into the influence of the particle size distribution on the powder bed fusion (PBF) bed density. Based on the simulation results presented by Xiang et al. [3], it has been observed that the powder packing density is greater in the case of a monosize distribution, compared to a Gaussian distribution, and that the powder packing density is further increased in the case of a bimodal size distribution. On the other hand, Jacob et al. [4,5], in their experimental works, showed that the dispersion of a powder with a broader range of particle sizes can lead to the formation of a compact powder bed. This phenomenon primarily occurs due to the ability of smaller particles to occupy the interstitial spaces between larger particles. Chen et al. [6] conducted a simulation that showed that an increased ratio of fine particles within the bulk powder leads to the agglomeration of the powder and, subsequently, results in a reduction in the density of the powder bed. Additionally, the experimental results of Muiz-Lerma et al. [7] show that the density of the powder bed is higher when powders with narrow particle size distributions are used, compared to powders with wide particle size distributions [8]. According to the DEM simulation findings of Ma et al. [9], the introduction of a small quantity of fine particles results in a decrease in the overall volume of voids within the powder bed. In the simulation, when the concentration of fine content exceeded 1.5 percent, there was a reduction of 5.6 percent in the volume fraction of solid material, compared to the baseline composition [10]. The simulation results of Yao et al. [11] show that the inclusion of a significant number of fine particles in powder blends leads to an increased relative density in the powder bed. In addition to the particle size distribution, another factor affecting the density of the powder bed concerns the spreader machine settings, such as the spreader velocity, type, and gap thickness. However, the relationship between these factors, and their combined impact on the powder bed quality remains relatively unexplored, highlighting the need for further investigation, to establish comprehensive guidelines for optimising the spread-layer quality in powder additive manufacturing.

The findings from a significant number of experimental studies and discrete element method (DEM) simulations have consistently shown a decrease in the density of the powder bed when the spreader velocity is high. The simulation results presented by Zang et al. [12] demonstrated that an increase in bed density was achieved when the translational velocity of the roller was decreased. According to the simulation findings reported by Desai and Higgs [13], there was an observed increase in the "layer porosity" of the powder as the speed of the recoater increased. Yan et al. [14] and Meier et al. [15] conducted simulations and found that the "packing density" of the powder beds decreased as the spreader speed increased. The simulation results conducted by Chen et al. [6] demonstrated that there was an increase in the number of "empty patches" within the powder bed when the velocity of the roller spreader was increased from 10 to 500 mm/s. According to the simulation findings of Yao et al. [11], the powder bed showed a larger "volume of pore space around the particle" when the spreader velocity increased. According to the findings of Lee et al. [16], simulation results indicated a decrease in the packing density of the powder bed by approximately 5% when the spreader velocity was increased by a factor of 5. The findings presented by Fouda and Bayly [17] indicated that the overall packing bed fraction declined from 47% to 25% as the spreader velocity increased from 10 mm/s to 100 mm/s, as observed in the simulation results. The study conducted by Snow et al. [18] investigated the impact of the recoater blade spreader velocity on the percentage of the build plate covered by the spread powder. Two levels of velocity were examined, namely

50 and 150 mm/s. In the conducted experimental study, it was observed that the velocity of the spreader did not have any discernible effect on the proportion of the build plate that was covered by the spread powder.

The findings regarding the spreader velocity, and its impact on the powder bed density, provide valuable insights into optimising the spread-layer quality. However, in addition to the spreader velocity, other factors, such as the spreader shape and gap thickness, have also been observed to influence the powder bed density. According to Yan et al. [14], the design of the spreader has no effect on the powder bed packing fraction at low translational speeds. In accordance with the findings of Haeri et al. [19], the utilisation of a roller spreader, as opposed to a blade spreader, leads to a greater level of bed density. In a separate study, Haeri [20] found that at a low translational spreader velocity, the powder bed volume fraction achieved by an elliptical shape blade is slightly lower than the powder bed volume percent achieved by a roller spreader. Conversely, a contrasting pattern was observed at higher speeds of dispersion.

The gap size, which refers to the distance between the recoater and the build plate, is a crucial factor that influences the density of the powder bed. Based on the findings of the simulation results of Yao et al. [11], it was observed that the packing density of the powder bed increased as the gap height increased, up to a specific threshold. However, once this threshold was surpassed, the gap height no longer had any discernible impact on the density of the powder bed. Based on Fouda and Bayly's simulation results [17], it was observed that the overall bed packing fraction of the powder bed exhibited a nearly linear increase, ranging from 15% to 33%, as the gap thickness expanded, within the range of 0.01–0.03 mm. Based on the findings reported by Meier et al. [15], in order to get a 'continuous powder layer', the gap height for a 'cohesive' powder should be 3 to 4 times larger than the powder's D_{90} value. In order to achieve a continuous layer of powder, it is necessary for the gap height to be twice the size of the D_{90} of the powder, with a lower cohesion. Han et al. [21] found, in their simulation results, that when spreading occurs at a gap size higher than the bulk powder average particle diameter (16% or 45%), it leads to the formation of a homogeneous first layer powder bed. According to the findings of Zang et al. [12], simulation results showed that when the gap size is within the same range as the tested powder's D_{50}, it results in a significantly reduced density in the powder bed. In order to attain a uniform powder bed, the authors suggested employing a gap size that is three times larger than the D_{50} of the powder.

In addition to considering the powder bed density, it is crucial to comprehend the variations in particle size and shape within the powder bed fusion (PBF) build plate. This understanding is vital for the optimisation of the powder bed quality, and the mitigation of size segregation phenomena. The use of DEM simulations has facilitated a comprehensive investigation, yielding valuable insights regarding the distribution of particle sizes, and the prevalence of size segregation, within the powder bed. Nevertheless, it is imperative to conduct empirical studies to examine the phenomenon of size and shape segregation on the build plate. Mussatto et al. [5] found that metal powders with a broad range of particle sizes, and a substantial percentage of particles smaller than 25 μm, exhibited a higher susceptibility to size segregation within the powder bed. As per the findings of Nan et al. [22], it has been observed that the accumulation of powder behind the blade recoater is characterised by a greater concentration of larger particles. This phenomenon, referred to as size segregation, occurs due to the tendency towards jamming at smaller gap sizes. In a study conducted by Jacob et al. [4], it was observed that the particle size of the powders being tested exhibited an evident increase within the powder collecting bins, suggesting a distinct phenomenon of size segregation. In addition, it has been observed that larger particles exhibit a tendency to accumulate in close proximity to the dispenser side, specifically at the end location of the powder bed build plate. According to the findings of Muiz-Lerma et al. [7], it was observed that the powder bed exhibited larger particles during the initial stages of the powder spreading process. On the other hand, the powder bed in close proximity to the collection point exhibits a higher concentration of smaller particles.

However, Lee et al. [16] and Chen et al. [6] used the DEM, and found that the proportion of large particles increased in the direction of the blade recoater during spreading.

This study offers an original and thorough examination of the variables that impact the quality of the spread layers in powder additive manufacturing, with specific emphasis on the crucial factors of the packing fraction and the segregation tendency. Previous studies have primarily used simulation methods with limited experimental validations. However, this research aims to address this gap, by conducting comprehensive experimental investigations. The majority of research conducted utilising the discrete element method (DEM) has employed contact models that exhibit significant simplifications, in comparison to the complex nature of real particulate material systems. Specifically, the simulations are conducted using uniform spherical particles arranged in a structured packing, while the actual system consists of particles with varying sizes, each possessing a unique shape, all of which are angular in nature. Furthermore, these particles are packed together in an extensive range of diverse juxtapositions, almost infinite in nature.

This study offers valuable insights and clarifications, by investigating the effects of the particle size distribution, spreader machine settings (such as the velocity, shape, and gap thickness), and variations in the particle size and shape. The results of this study will make a valuable contribution towards the optimisation of the powder bed density, and improvements in the overall quality of the 3D-printed components. This paper will address significant gaps in the existing body of knowledge, and advance the field of powder additive manufacturing.

2. Spreader Test Rig

In order to study the relative packing fraction, and the segregation tendency of the powder bed in the AM process, a new spreader tester was designed and developed at the Wolfson Centre for Bulk Solids Handling Technology. The details of the tester was described in detail by Salehi et al. [1]. The spreadability testing setup is shown in Figure 1, together with all of its features. The close-up mechanical details of the recoater blade control parts are presented in detail in Figure 2. The features of the drive arrangement for the horizontal (spreading) motion are shown in Figure 3.

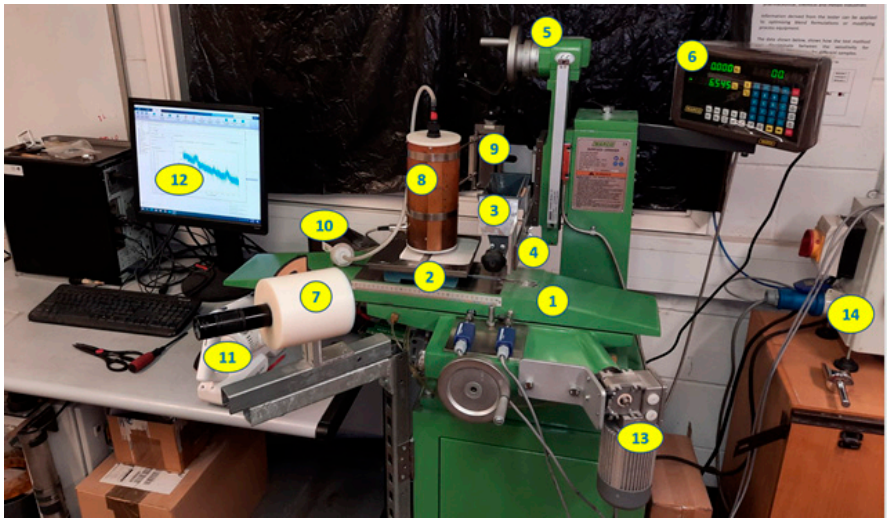

Figure 1. The AM powder spreadability tester based at the Wolfson Centre: 1. commercial machine frame for x-y-z motion; 2. spread table on a moving carriage; 3. powder dispenser; 4. spreader blade; 5. blade-table clearance adjustment; 6. blade-table clearance digital readout; 7. collimated light source (not used in this paper); 8. electrostatic sensor (not used in this paper); 9. height adjuster for the electrostatic sensor (not used in this paper); 10. powder filter (not used in this paper); 11. vacuum source (not used in this paper); 12. computer for data logging (not used in this paper); 13. motor drive for the carriage; and 14. controller for the carriage drive.

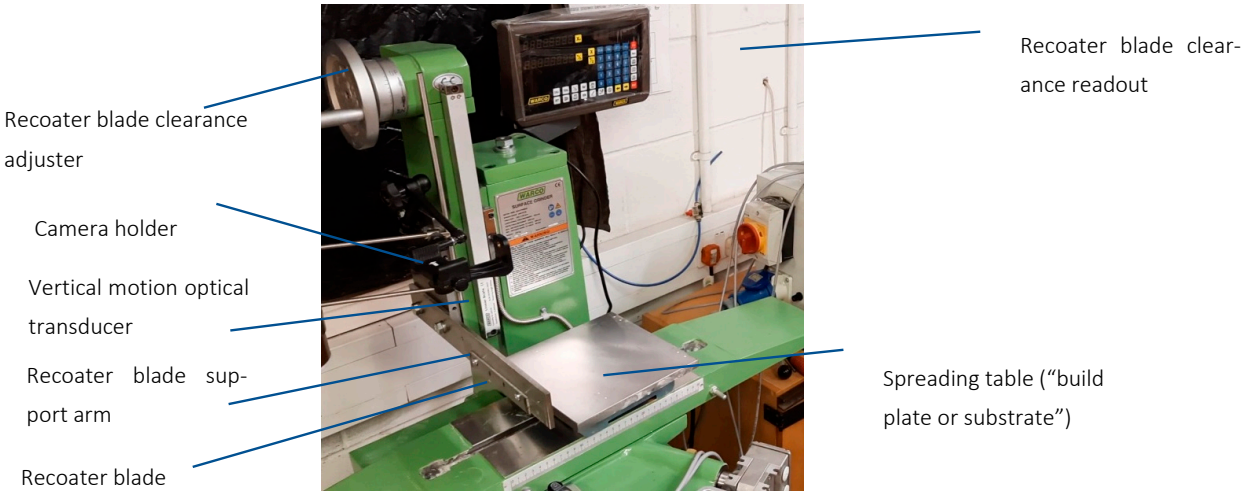

Figure 2. Close-up of the mechanical details of the recoater blade control elements.

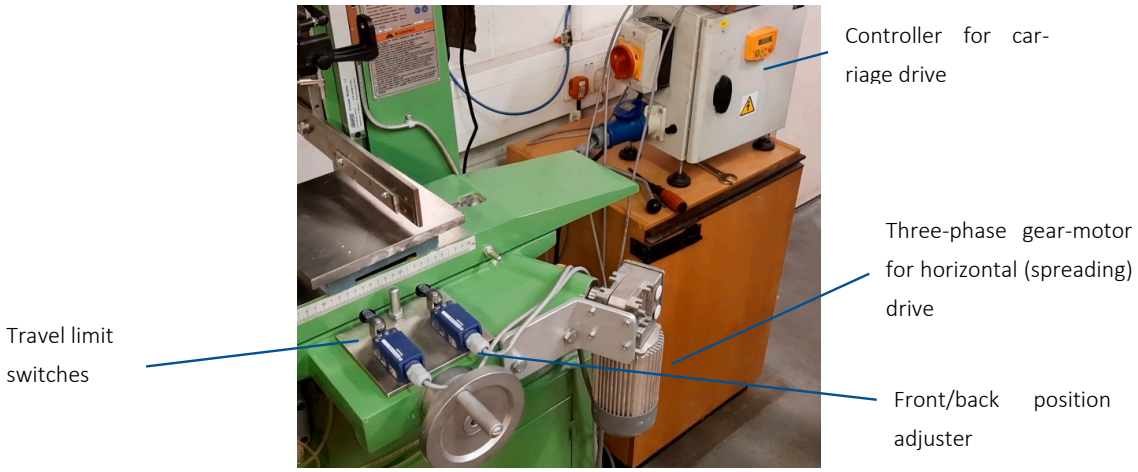

Figure 3. Details of the drive arrangement for a horizontal (spreading) motion.

2.1. Powder Deposition System

Powder deposition requires a dependable and repeatable procedure. This would need to be capable of depositing a known, regulated volume of powder uniformly across the width of the substrate, in front of the recoater blade. The deposition device developed by the Wolfson Centre consists of a hopper filled with powder, positioned above a cylindrical shaft with a diameter of 16 mm. The shaft features a slot that is 5 mm wide and 5 mm deep (see Figure 4a–d).

The hopper side plates were manufactured using steel, to reduce the adherence of particles due to electrostatic charge. The rotor and stator were manufactured from acetal and PVC, respectively.

2.2. Powder Spreading ("Recoater") Blades

In this investigation, two alternative recoater blade geometries were used. Figure 5 depicts the sketches of the two recoaters. Figure 5a shows a recoater with a larger cross-sectional area and a flat "nose", which is referred to as recoater configuration 1, or NB, in this paper. Figure 5b shows a tapered recoater with a lower cross-sectional area and a sharp edge, which is referred to as recoater configuration 2, or IB. According to Meier et al. [15], for a cohesive powder, the gap height should be 3 to 4 times greater than the powder's D_{90}, in order to achieve a 'continuous powder layer'. To get a 'continues powder layer', the gap height for the 'less cohesive' powder must be twice as large as the powder's D_{90}. As a

result, two reasonable gap thicknesses were chosen: two times larger than the powder's D_{90}, and five times larger than the powder's D_{90}.

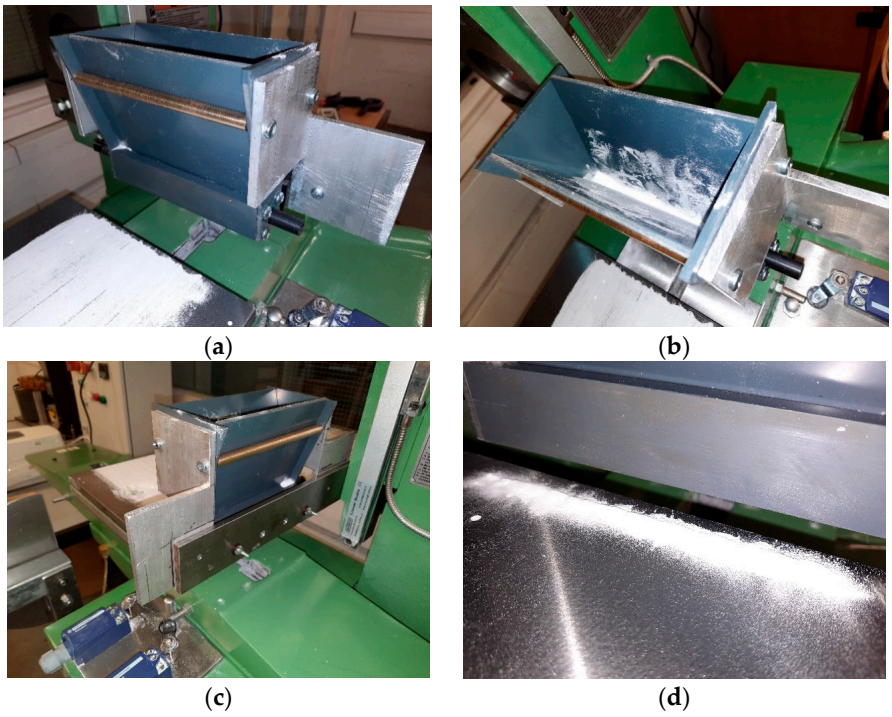

(**a**) (**b**) (**c**) (**d**)

Figure 4. The powder deposition system: (**a**) the side; (**b**) the top view; (**c**) the attachment of the powder deposition unit on the recoater blade support bar; and (**d**) an example of the controlled quantity of powder deposited in a single turn of the rotor.

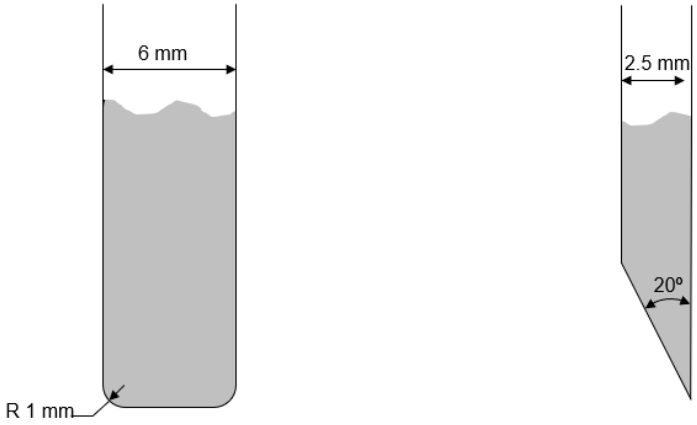

(**a**) (**b**)

Figure 5. The two tested recoater shapes: (**a**) recoater configuration 1 or NB; and (**b**) recoater configuration 2, tapered blade, or IB.

2.3. Powder Bed Density Measurements

The powders were gathered from the powder bed in close proximity to both the deposition point and the collection point, utilising two square compartments. These compartments were open at the top and bottom, with a narrow edge running along the base of the walls (see Figure 6a). The size of the compartment's side was 45 mm. A dead weight was placed over each compartment. Subsequently, the powder located on the exterior of each compartment was gently removed by brushing. The measurement of the mass of powders in each compartment was conducted (see Figure 6b). Given the assumption that

the height of the powder layer above the powder bed was equivalent to the size of the gap between the recoater, it became possible to compute the volume of powder contained within each compartment. The ability to determine the powder bed density was facilitated by knowledge of the mass of powder contained within each compartment.

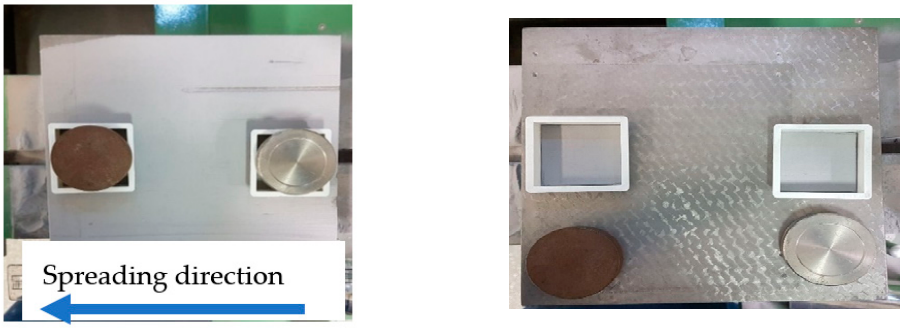

(**a**) (**b**)

Figure 6. The powder bed density measurement procedure.

3. Materials

Six different polymer powders were supplied by the Ricoh Company, and were used in this research work

- Ricoh polypropylene (PP), a spherical particle shape produced by melt emulsification.
- PP2—a polypropylene powder produced using cryogenic milling (cornflake particle shape).
- TIGITAL® SERIES 371 PREMIUM PERFORMANCE (Tiger Coatings), a thermoset powder produced through milling. Referred to as Thermoset in the text.
- Polybutylene terephthalate (PBT), a powder characterised by cylindrical powders, produced through a patented Ricoh process named EMIC (Extended Fibre Micro Cut), which consists of chopping polymer fibres with a very controlled particle size and shape. Referred to PBT in the text.
- PA2200 (PA12)—nylon 12 produced through precipitation (with a "potato-like" shape in particles), the most common material for powder bed fusion technologies (around 80% of the market).
- Ricoh PA6 GB—a mix of nylon 6 powder (produced through cryogenic milling) + 40% glass beads.

Six different metal powders, with more spherical particles compared to the polymer powders, were also tested:

- LPW-TI64-GD23-41-GR1-12232
- LPW-TI64GD23-41-UK84996
- LPW-TI64GD23-41-GR1-12455
- LPW-TI64GD23-AAFD-UK3324 (TI)
- ALSI10MG LPBF FLEXIBLE-BATCH PR100341
- LPW-ALSI10MG-28-GR1-12412 (AL)

4. Powder Characterisation

4.1. Flow Function

The Brookfield powder flow tester (PFT) was used to determine the flow properties of the powders [23]. The tester's operation and extensive descriptions have been published elsewhere [24]. The number of consolidation points (i.e., the yield loci) and over-consolidation points (i.e., the points in each yield locus) were set to four and five, respectively. Jenike describes the technique for extracting the flow parameters of powders from the shear tester in detail [25]. A typical approach to reporting powder flowability is the Jenike flowability classification, using the flow function value, $ff_c = \sigma_1 / f_c$. The classes generally considered are the free flowing ($ff_c \geq 10$ or $1/ff_c < 0.1$), easy flowing ($4 < ff_c \leq 10$

or $0.1 < 1/ff_c < 0.25$), cohesive ($2 < ff_c \leq 4$ or $0.25 < 1/ff_c < 0.5$), very cohesive ($1 < ff_c \leq 2$ or $0.5 < 1/ff_c < 1$) and non-flowing ($ff_c \leq 1$ or $1/ff_c > 1$).

The unconfined yield strength, as a function of the major principal stress for all the tested powders, is depicted in Figure 7 for plastic powders, and Figure 8 for metal powders. The unconfined failure strength, calculated using (1), is a combined function of the friction angle, φ_i, and the powder cohesion, c. Hence, the results of the bulk cohesion and friction angle were not reported.

$$f_c = 2c\frac{\cos\varphi_i}{1-\sin\varphi_i} \quad (1)$$

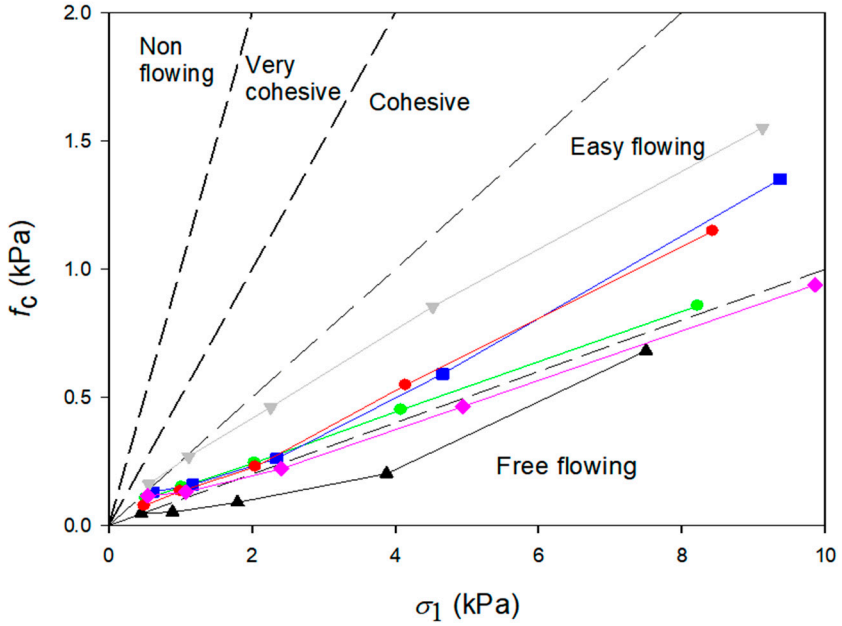

Figure 7. The flow function of the tested plastic powders: PP2 (■); Ricoh-PP (▲); Thermoset (▼); PBT (●); PA6 (♦); and PA2200 (●).

When the results of the plastic powders were compared, all the powders except PA6 and Ricoh PP were classed as easy-flowing powders. Ricoh PP was the most free-flowing powder, compared to the other plastic powders. The flow function of all the metal powders is classified as a free-flowing powder, with a slight tendency towards the easy-flowing region at a low consolidation stress.

4.2. Tap Density

In order to measure the loose bulk density, ρ_t, the powders were poured to overfill a cylindrical container with a known volume. Afterwards, the container was tapped 1500 times, and then the weight of the powder, and the volume of the powder inside the container were recorded.

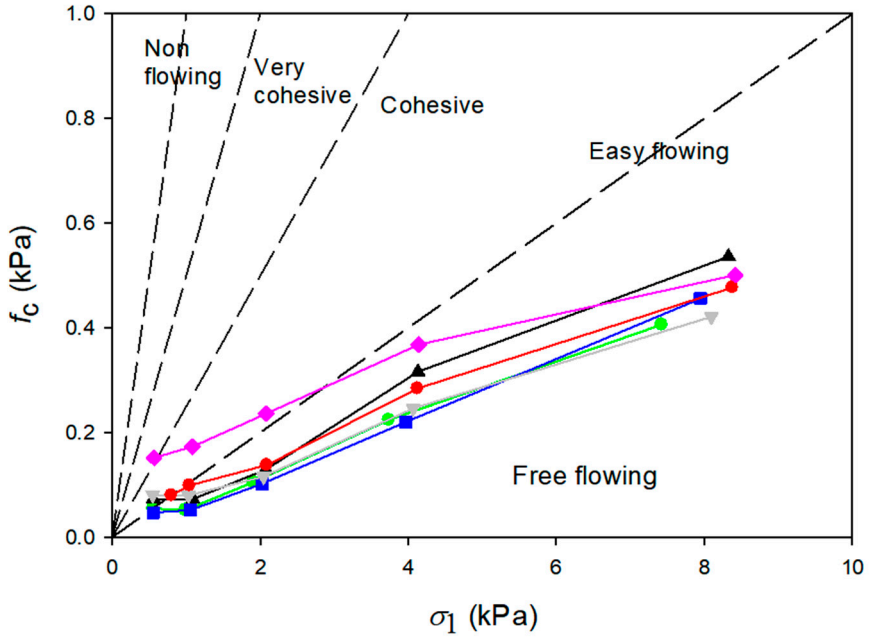

Figure 8. The flow function of the tested metal powders: LPW-TI64GD23-41-GR1-12455 (■); LPW-TI64-GD23-41-GR1-12232 (▲); LPW-ALSI10MG-28-GR1-12412 (▼); LPW-TI64GD23-41-UK84996 (●); LPW-TI64GD23-AAFD-UK3324 (♦); and ALSI10MG LPBF FLEXIBLE-BATCH PR100341 (●).

4.3. Particle Size Distributions

The particle size distribution was measured using a laser diffraction particle size analyser (Malvern, Mastersizer Sirocco 2000), with Sirocco dry powder feeder, and using dry air as the dispersion medium. The data derived from the Mastersizer are presented in Table 1. The powder size span of a volume-based size distribution is defined as = $(D_{90} - D_{10})/D_{50}$.

Table 1. The particle size distribution of the tested powders.

Material	D_{10}	D_{50}	D_{90}	Size Span
	(μm)	(μm)	(μm)	(-)
Ricoh PP	28	49	85	1.16
PP2 PTD03	42	84	139	1.15
Digital thermoset	15	44	80	1.47
PBT	52	70	95	0.59
Ricoh PA6 GB	19	65	111	1.41
PA2200	35	52	72	0.711
LPW-ALSI10MG-28-GR1-12412	27	50	83	1.12
LPW-TI64GD23-AAFD-UK3324	15	27	42	1
ALSI10MG-LPBF-FLEXIBLE	20	41	65	1.1
LPW-TI64GD23-41-GR1-12455	15	27	42	1
LPW-TI64GD23-41-UK84996	17	28	44	0.96
LPW-TI64-GD23-41-GR1-12232	14	30	40	0.86

4.4. Particle Shape

The SEM images of the tested powders are depicted in Figure 9. The thermoset and PP2 have irregularly shaped particles, PBT has the cylindrical particles, Ricoh-PP has spherical and oval-shaped particles, and the metal powders have more spherical particles. Among the metal powders, ALSI10MG LPBF has more elongated/irregular particles, compared to the other tested metal powders.

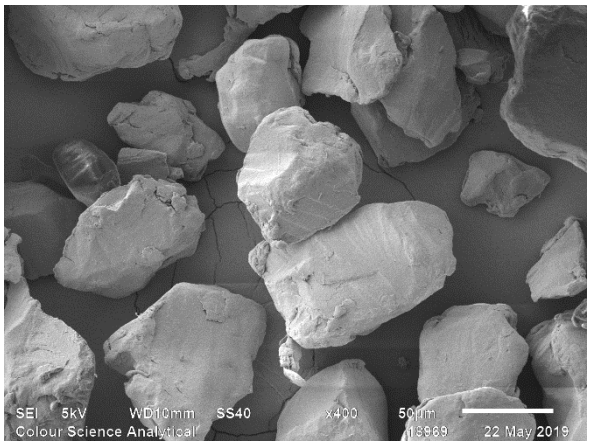

(Thermoset)

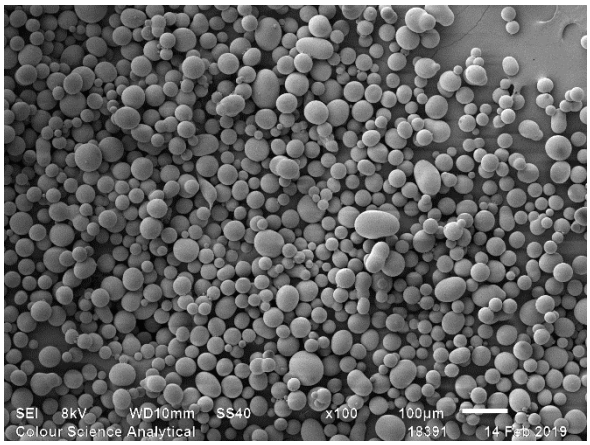

(Ricoh PP)

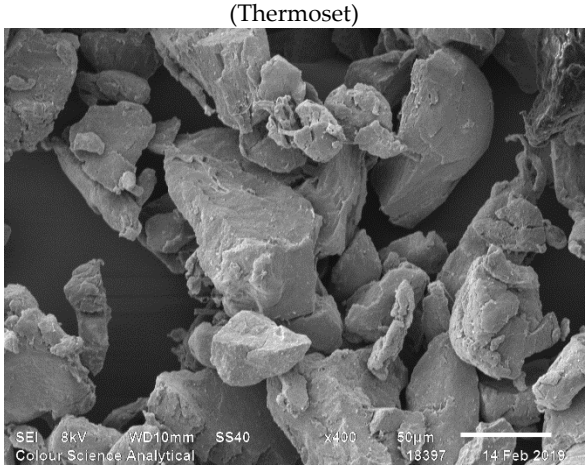

(PP2)

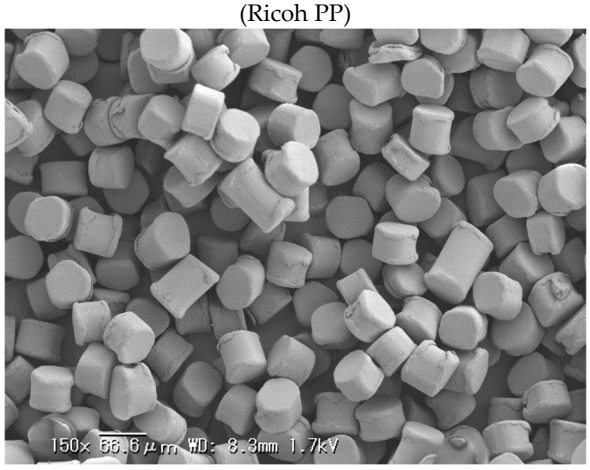

(PPT)

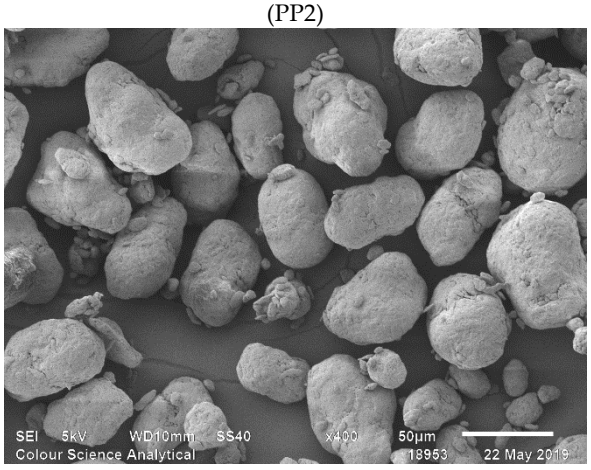

(PA2200)

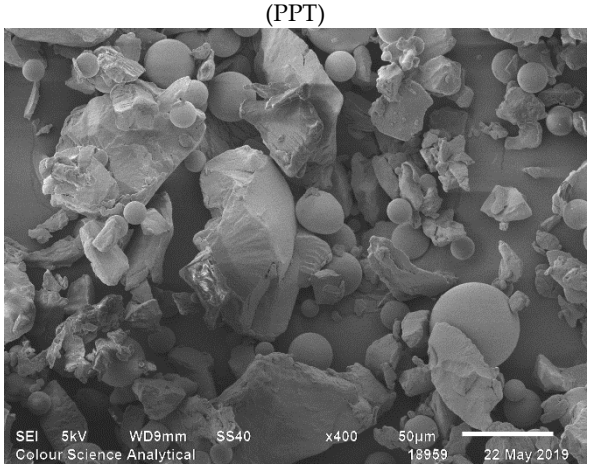

(PA6 GB)

Figure 9. *Cont*.

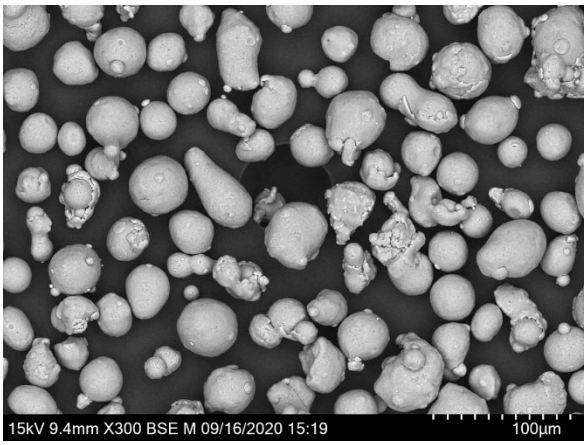

(ALSI10MG LPBF FLEXIBLE)

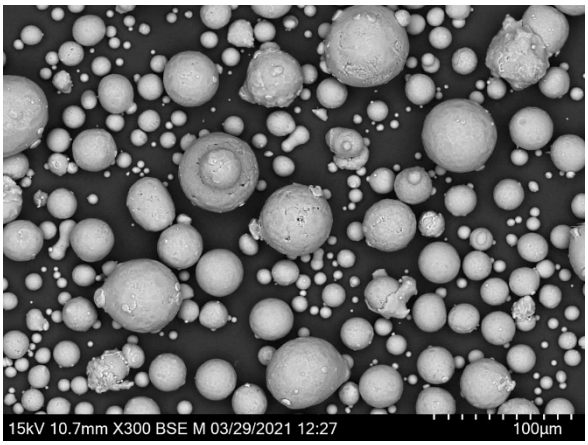

(LPW-ALSI10MG-28-GR1-12412)

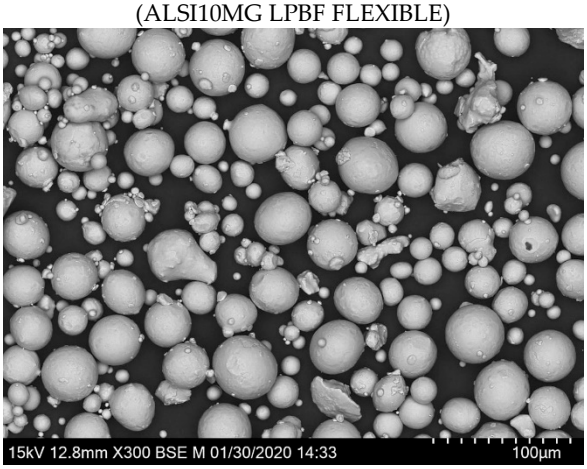

(LPW-TI64-GD23-41-GR1-12232)

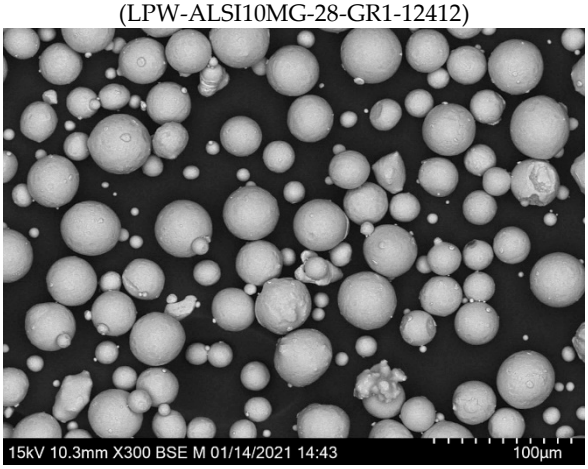

(LPW-TI64GD23-41-GR1-12455)

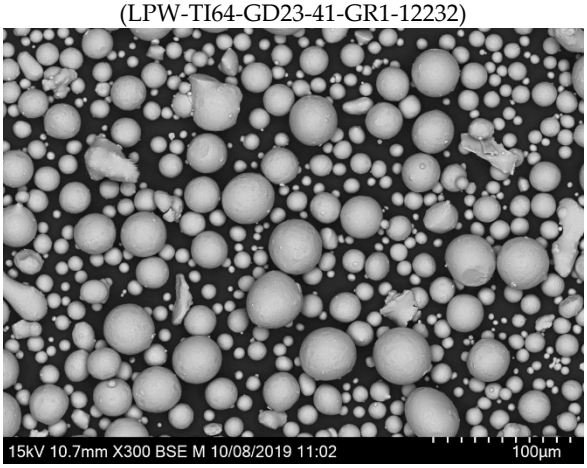

(LPW-TI64GD23-41-UK84996)

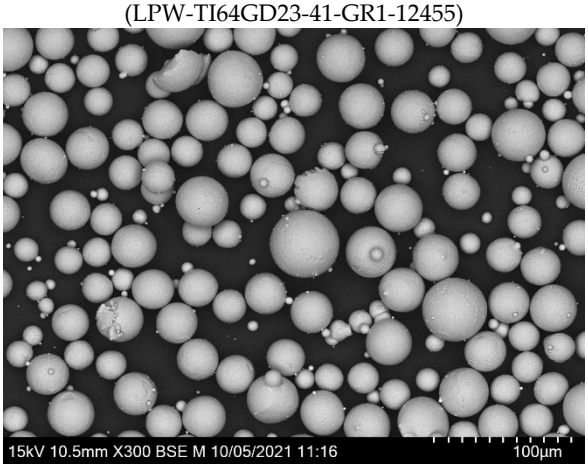

(LPW-TI64GD23-AAFD-UK3324)

Figure 9. Microscopic images of the tested powders.

4.5. Particle Size and Shape Analysis with G3 (Used for the Segregation Studies)

The G3 morphology was used to evaluate the particle size distribution, as well as the elongation index (aspect ratio) of the powders collected from location 1 and 2 in the build plate (near the deposition and collection points, respectively). The data derived from the G3 are presented in Table 2.

Table 2. The particle size distribution and elongation index of the virgin powder and spread powder at the collection points 1 and 2 on the powder build plate. The gap size is set to 2*D_{90}. Both recoater shapes were tested. 1L: location 1, near the deposition point. 2L: location 2, near the collection point.

		D_{10} (µm)	D_{50} (µm)	D_{90} (µm)	Elongation Index (µm)
PP2					
	Virgin	69.39	109.7	175.8	0.364
	IB1L	70.72	119.9	192.2	0.368
	IB2L	73.49	114.4	178.2	0.376
	NB1L	71.2	102.9	136.1	0.159
	NB2L	69.44	111.1	181	0.221
Thermoset					
	Virgin	32.16	61.64	99.84	0.242
	IB1L	32.64	61.68	95.79	0.40
	IB2L	39.21	72.65	95.29	0.14
	NB1L	35.51	61.16	95.3	0.43
	NB2L	37.24	70.33	115.4	0.25
PBT					
	Virgin	63.5	74.71	112.3	0.227
	IB1L	64.29	77.46	116	0.224
	IB2L	67.3	91.9	125.1	0.363
	NB1L	63.7	69.5	77.66	0.105
	NB2L	65.96	92.25	124.3	0.350
ALSI10MG LPBF					
	Virgin	27.78	48.64	61.02	0.110
	IB1L	29.18	50.21	64.79	0.116
	IB2L	30.95	51.03	68.26	0.119
	NB1L	27.34	49.87	62.26	0.112
	NB2L	27.55	49.75	61.40	0.113
Ricoh PP					
	Virgin	38.09	71.08	128	0.156
	IB1L	38.74	69.07	133.3	0.151
	IB2L	51.68	81.32	131.1	0.356
	NB1L	31.58	45.8	84.57	0.342
	NB2L	51.5	81.14	131	0.353
PA6 GB					
	Virgin	45.15	93.1	170.7	0.208
	IB1L	42.43	93.84	176.9	0.108
	IB2L	51.3	101	197.8	0.243
	NB1L	43.1	89.44	179.8	0.080
	NB2L	40.23	93.5	180.9	0.085
PA 2200					
	Virgin	52.47	79.8	120	0.225
	IB1L	57.4	91	144	0.275
	IB2L	59.27	95.6	155.2	0.275
	NB1L	54.09	73.15	120.7	0.154
	NB2L	53.66	84.5	124.2	0.283
LPW-TI64GD23-41-GR1-12455					
	Virgin	15.70	27.50	42.14	0.105
	IB1L	16.20	29.04	51.28	0.110
	IB2L	17.02	30.57	53.44	0.114
	NB1L	15.95	28.15	50.02	0.107
	NB2L	16.52	29.04	49.8	0.109

5. Results and Discussion

The powders that were studied have different bulk and tapped densities, which will result in different powder bed densities, making the comparison of the spreadability of the different powders difficult. Yan et al. [14] stated that the relative packing density would be an apocopate index to evaluate the powder spreading, as a more compacted powder

bed would normally be desirable for the fabrication quality. Later, Haydari [26] proposed that the results for the spreadability could be better evaluated using the ratio of the spread-layer bulk density to the initial bulk density of the powders. In her work, this ratio was defined as the "spreadability index". In the current study, to eliminate the aforementioned discrepancies from the comparisons, the powder bed densities of the tested powders were divided by both the powder's compacted bulk density (measured with the PFT under the low stress of 0.5 kPa), and the powder's tapped density.

Each measured powder has a very similar compacted bulk density and tapped density. As a result, when evaluating the tapped density, the relative packing fraction of the powder bed is close to the relative packing fractions, when considering the compacted bulk density. As a result, only the packing fraction results based on the compacted bulk density are presented in this work. The following data present the powder relative packing fractions (packing ratio) for two different gap sizes, 2*D_{90} and 5*D_{90}, as well as two sampling points within the powder bed. Sampling point 1 is located near the deposition point, while sampling point 2 is near the collection point of the excess powder. The recoater shapes used for the measurements are IB and NB.

5.1. Relative Packing Fraction (Ratio) at the Gap Size 5*D_{90}

The results of the relative packing fraction (powder bed density/bulk density) for the Ricoh plastic powders are reported in Figure 10, and those for the metal powders are reported in Figure 11, both spread at the gap size five times higher than the powder's D_{90}. The circular symbols (●, ○) represent the relative packing fraction using the NB recoater. The rectangular symbols, (■, □) represent the relative packing fraction using the IB recoater. The filled symbols (■, ●) represent the powder relative packing fraction near the deposition point (sampling point 1), and the empty symbols (○, □) represent the relative packing fraction near the collection point (sampling point 2). The error bars in all figures represent the standard deviation from three repetitions (four tests in total).

For both the plastic and metal powders spread at the gap size of 5*D_{90}, a higher relative packing fraction is obtained when using NB (wide nose), compared to the IB (sharp edge) recoater. This is likely attributed to two effects, as follows.

The NB (wide nose) recoater has a radius on the leading edge, which would tend to apply a downwards force to the particles as they pass under the edge of the blade. Zhang et al. reported that a larger roller diameter leads to a larger compression zone in the powder bed, and hence provides a higher bed density [12]; this might be also the case for the blade recoater.

Moreover, this recoater has a flat surface held above the particles for several millimetres of travel after they pass under the leading edge, helping to settle the particles, and prevent them from rotating and "flipping" upwards, which they can do with a sharp edge once it passes.

More in-depth research is certainly needed into the details of the recoater blade profiles, particularly the importance of a leading edge radius and a flat, level (or potentially slightly descending) surface behind the leading edge, to assist in packing, stabilising, and possibly densifying the particles. However, it is known that there is uncertainty over the question of how high a packing density is desirable from a processing perspective, so these issues should ideally be investigated hand-in-hand. Particularly, the powder thermal conductivity [27] is an important bulk property affecting the quality of the final artefacts. Sillani et al. [27] reported that there is a positive association between the powder bed packing density and the powder conductivity. They discovered that increasing the powder bed packing density (attained through compaction) from 0 to 100% increases the powder thermal conductivity by 10 to 40%. These points deserve more investigation, and the authors plan to carry out additional research into them.

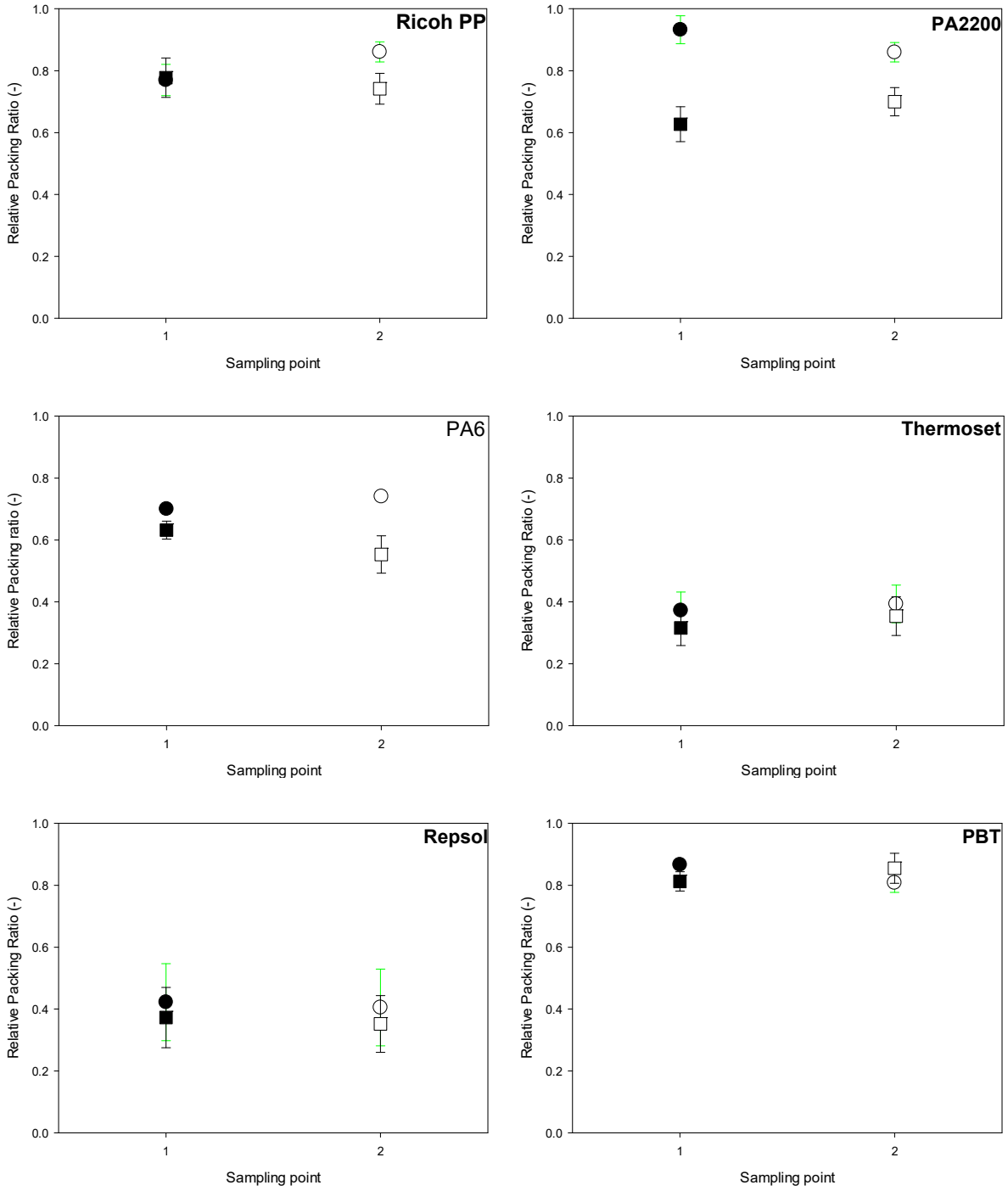

Figure 10. The relative packing fraction (relative packing ratio) of the tested plastic powders at the reacoater gap size five times higher than the powder's D_{90} (measured using the Malvern Mastersizer). Sampling number 1: near the deposition point, and sampling point 2: near the collection point. NB recoater (●, ○); IB recoater (■, □). The error bars are the standard deviation derived from four tests.

Jacob et al. [28] found that the powder bed density was slightly higher in the build plate towards the powder collector, than on the dispenser side. We also identified a consistently higher relative packing fraction near the collection point (sample point 2) when using the NB recoater, with the exception of the PA2200 and PP2 powders. PP2 is more cohesive than the other powders evaluated. This could explain the disparity in the PP2 powder's trend. PP2 and Thermoset have the lowest bed density of the powders examined, which coincides with their higher $1/ff_c$ values (more cohesive). A low bed

density is caused by a high particle cohesiveness between particles, between particles and the recoater, and between particles and the build plate. The powder bed for these two powders is much less homogeneous, due to their reduced density. Figure 10 also shows a greater variance between repetitions for both the PP2 and Thermoset powders, compared to the studied free-flowing plastic powders, namely Ricoh-PP and PA2200, presumably due to their poorer flowability.

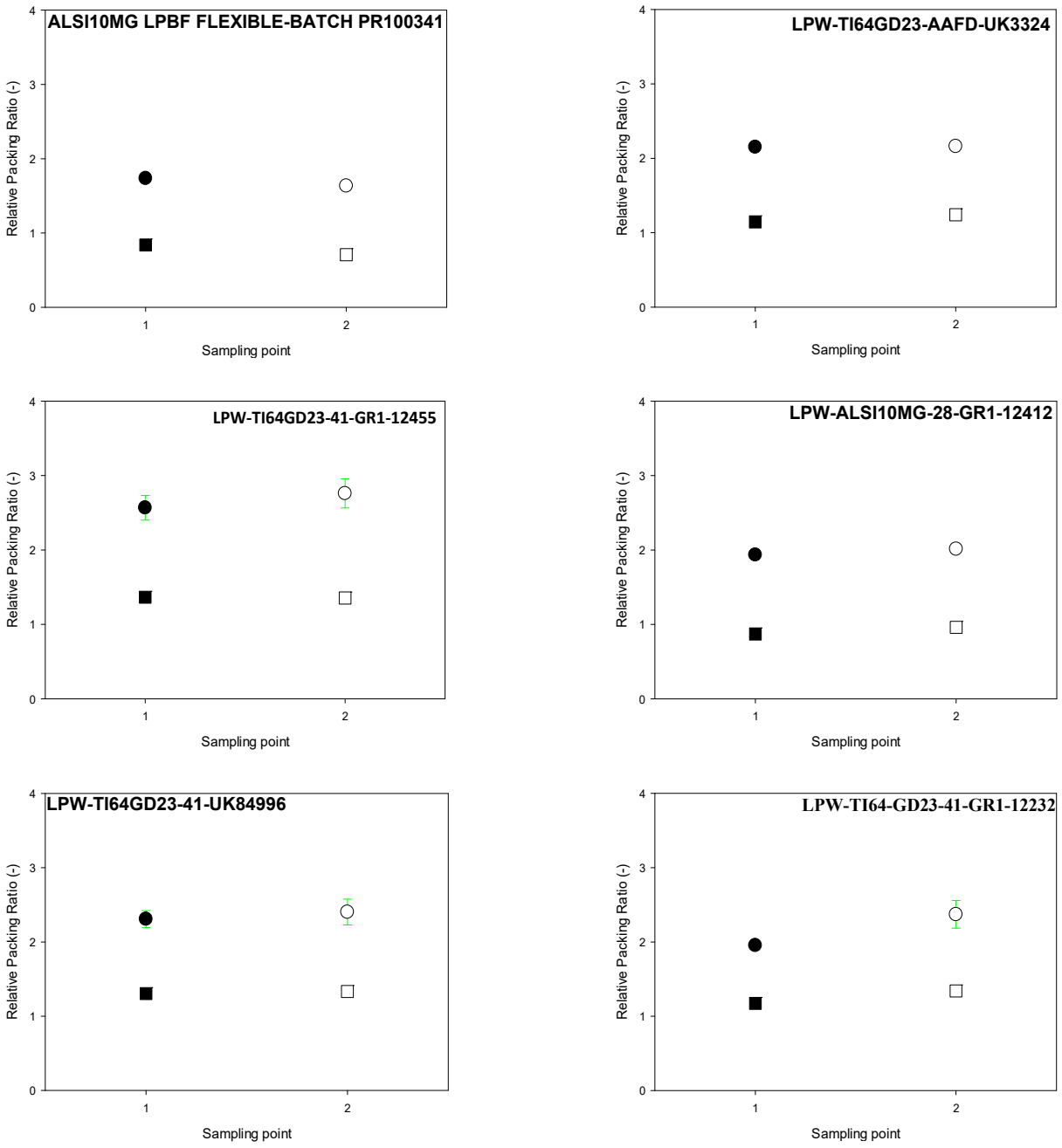

Figure 11. The relative packing fraction (relative packing ratio) of the tested metal powders at the reacoater gap size five times higher than the powder's D_{90}. Sampling number 1: near the deposition point, and sampling point 2: near the collection point. NB recoater (●,○); IB recoater (■,□). The error bars are the standard deviation derived from four tests.

None of the plastic powders' bed-packing fractions attained a value of one. The most cohesive plastic powders had the smallest relative packing fraction, which corresponds to their greater compressibility (more cohesive powders show a greater change in the bulk

density with stress when measured in a shear cell or compaction cell). PA2200 and Ricoh PP (lowest $1/ff_c$), on the other hand, showed the highest powder bed relative packing fraction. The highest packing fractions were attained with the PBT, which might be attributed to the cylindrical particle shape of this powder. Compared to powders containing spherical particles, a greater amount of powder with cylindrical particles can be dispersed across the build plate. Further study with other powders containing cylindrical particles should be conducted, to confirm this observation.

A much higher relative packing fraction is attained when spreading metal powders, compared to plastic powders. Metal has a larger density and weight, and is more slippery, but it has a lower surface energy, thus it will pack better simply under its own weight. So, in other words, it compacts itself even with no applied stress. A similar or slightly higher relative packing fraction is attained at sampling point 2, compared to sampling point 1, for all the tested metal powders.

The maximum relative packing fraction of the studied metal powders is achieved by spreading LPW-TI64GD23-41-GR1-12455 powder (which has more spherical particles and a narrow particle size distribution) with both the NB and IB at collection point 1 or 2. On the other hand, the lowest relative packing fractions are obtained by spreading ALSI10MG-LPBF-FLEXIBLE, which has a wider particle size distribution, and more elongated and irregularly shaped particles. Furthermore, the angle of internal friction of the LPW-TI64GD23-41-GR1-12455 powder is slightly lower than the angle of internal friction of the ALSI10MG-LPBF-FLEXIBLE powder. A low internal friction angle means that the particles flow easily over each other, allowing for a higher packing fraction. These might be the reasons for the differences in the relative packing fraction between these two metal powders.

Similar to the tendency seen in the plastic powders, the relative packing fraction achieved when employing NB is larger than the relative packing fraction while spreading powders with IB. The difference in the relative packing fraction of metal powders achieved with these two recoaters, on the other hand, is more noticeable than the difference in the relative packing fraction of plastic powders. It should also be noted that the powder beds made from metal powders are more uniform than the powder beds made from plastic powders. As a result, the standard deviation of the relative packing fractions for the metal powders was lower than for the plastic powders.

*5.2. Spreading Powders at the Gap Size 2*D_{90}*

The results of the relative packing fraction (powder bed density/compacted bulk density) for the metal powders are reported in Figure 12, and for the plastic powders are reported in Figure 13.

In general, for the plastic powders, lower relative packing fractions were attained when the gap size was reduced from five times higher than D_{90} to two times higher than D_{90}, as expected. This trend was not observed for the two most cohesive plastic powders, PP2 and thermoset. The relative packing fractions attained for PP2 and thermoset at the gap size 2*D_{90} were higher than the relative packing fractions attained at the gap size of 5*D_{90}. This can likely be attributed to the fact that a more uniform powder bed is attained when spreading these two cohesive powders at the gap size of 2*D_{90}, compared to the condition where spreading at 5*D_{90}. In particular, at the higher gap size, the larger particles and/or agglomerates tend to pass through the gap between the recoater and the build plate, and hence cause more defects over the build plate. This causes less powder to be deposited over the build plate at the higher gap size for these two cohesive plastic powders and, hence, lower packing fractions.

A higher relative packing ratio was achieved using the NB recoater for the plastic powders, similar to the gap size of five times D_{90}, but with more significant differences, compared to the gap size of five times D_{90}. In addition, except for Ricoh-PP spread with the IB recoater, the relative packing fractions for all the plastic powders somewhat increased at sampling point 2. Ricoh-PP has the largest relative packing fraction (spherical particles)

among the plastic powders, followed by PBT (elongated particles and a narrow particle size distribution).

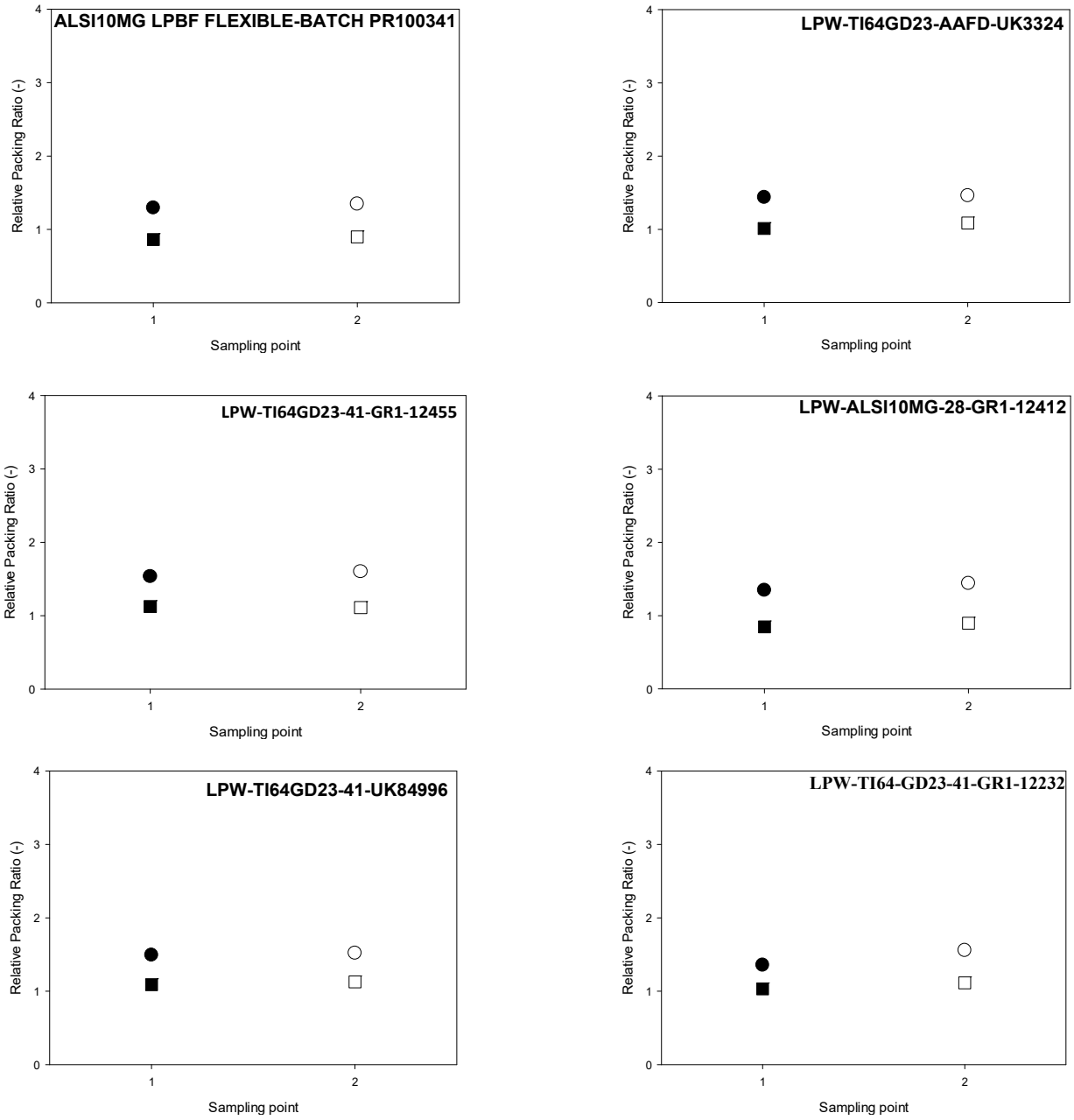

Figure 12. The relative packing fraction (relative packing ratio) of the plastic powders at the reacoater gap size of two times higher than the powder's D_{90}, both spread at the gap size two times higher than the powder's D_{90}. The circular symbols (●, ○) represent the bed density using the NB recoater. The rectangular symbols (■, □) represent the powder bed density using the IB recoater. The filled symbols (■, ●) represent the powder bed density near the deposition point (sampling point 1), and the empty symbols (○, □) represent the powder bed density near the collection point (sampling point 2). The error bars in all figures represent the standard deviation from three repetitions (four tests in total).

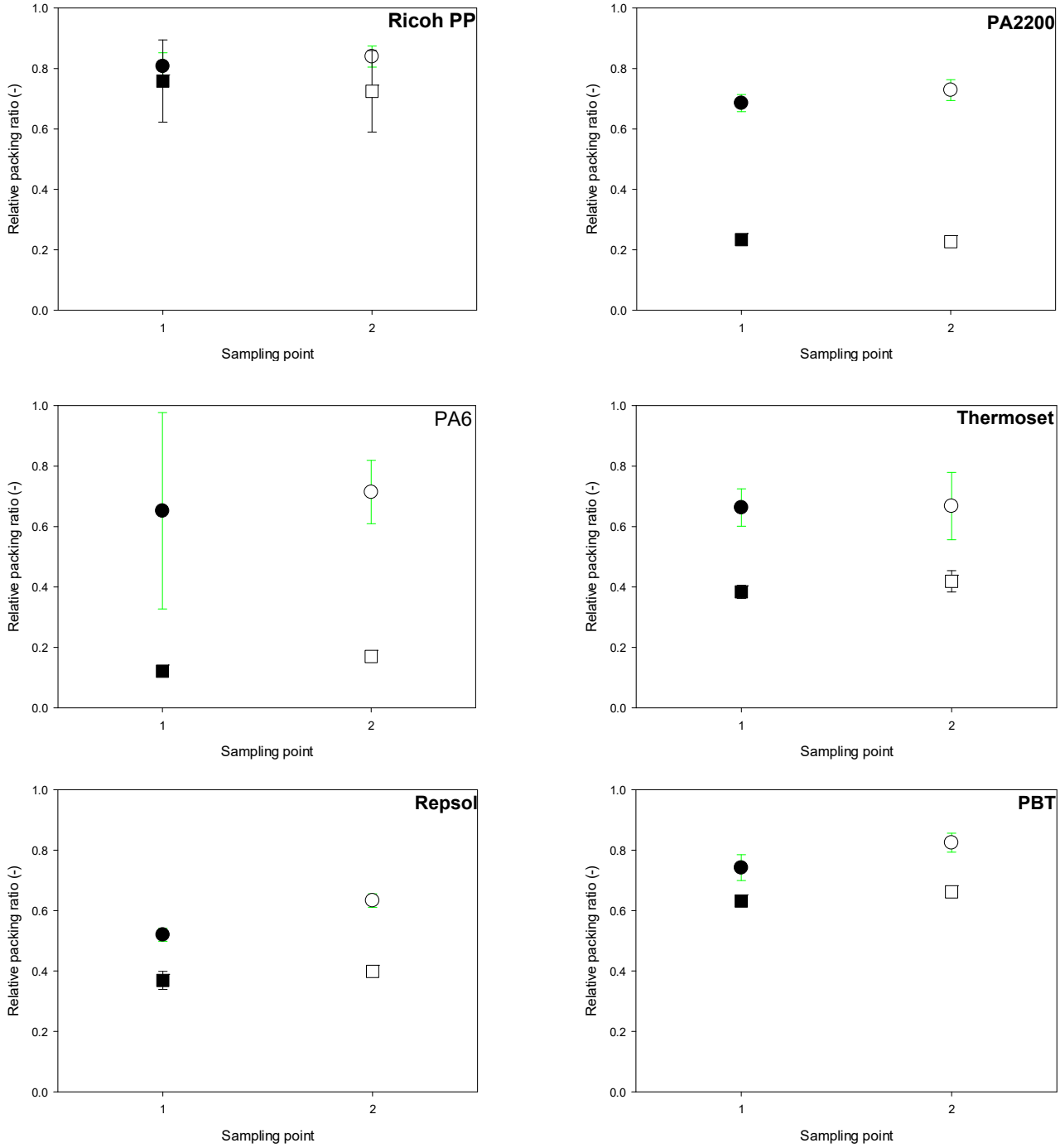

Figure 13. The relative packing fraction (relative packing ratio) of the plastic powders at the reacoater gap size two times higher than the powder's D_{90} (measured using the Malvern Mastersizer). Sampling number 1: near the deposition point; and sampling point 2: near the collection point. NB recoater (●, ○); IB recoater (■, □). Filled symbols (■, ●) represent the powder bed density near the deposition point (sampling point 1), and empty symbols (○, □) represent the powder bed density near the collection point (sampling point 2). The error bars in all the figures represent the standard deviation from three repetitions (four tests in total).

When comparing Figures 10 and 12, it was discovered that spreading plastic powders at smaller gap sizes resulted in a higher standard deviation in the relative packing ratio findings than spreading at larger gap sizes, especially for Ricoh-PP and PA6 GB. This could be due to increased transient jamming at smaller gaps [29].

The same relative packing fraction trend that was found at gap size 5*D_{90} was observed at gap size 2*D_{90}, where spreading metal powders resulted in a substantially larger relative packing fraction than spreading plastic powders. Additionally, a slightly higher packing fraction was observed at location 2, compared with location 1. Furthermore, the NB recoater provides a higher packing fraction, compared to the IB recoater. Similar to the trend observed at the gap size of 5*D_{90}, spreading LPW-TI64GD23-41-GR1-12455 powder with either NB or IB at either collection point 1 or 2 leads to the highest relative packing fraction, compared to the other tested metal powders. In contrast, the lowest relative packing fractions are attained when spreading ALSI10MG-LPBF-FLEXIBLE. This might be due to the narrow particle size distribution of this metal powder, compared to the other metal powders. Furthermore, Figure 9 shows that this powder contains more elongated particles, compared to the other tested metal powders.

5.3. Particle Size and Shape Segregation in the Powder Bed

These tests were conducted for all the plastic powders, and the two representatives of metal powders, ALSI10MG LPBF FLEXIBLE–BATCH PR100341 (aluminium-based powders) and LPW-TI64GD23-41-GR1-12455 (titanium-based powder). A small quantity of powder samples was taken from location 1 and 2, and then its size and shape were measured using the G3 morphology from Malvern. The size and shape segregation experiments were only conducted for the powder beds attained from the recoater gap size of 2*$D_{90,}$ due to the suspected higher tendency of the powder bed to undergo segregation because of jamming at the lower powder bed gap thicknesses.

The D_{10}, D_{50}, D_{90} and elongation index of the virgin powders (not spread), as well as the samples of powders from locations 1 and 2 spread with both the IB and NB recoaters, are summarized in Table 2. The results showed that the powder bed contains a higher fraction of finer and more rounded particles near the deposition point (sampling location 1), compared to the powder bed near the collection point (sampling location 2). The distribution of particle size could plausibly be attributed to the greater tendency of larger particles to jam between the spreader and build plate, as well as the particle percolation tending to allow both smaller and more rounded particles to drift towards the bottom of the moving heap in front of the blade.

The elongation index is higher at the second collection point; more rounded particles are deposited at location 1 (near the deposition point). Additionally, the elongation index is smaller when using the NB recoater, compared to when using the IB recoater, except for the Ricoh-PP in location 1. This might explain the lower relative packing fraction when using IB, compared to NB. This tendency does not follow for Thermoset. Thermoset is the most cohesive powder. A higher cohesion between particles is well known to lead to a lower segregation tendency in the powder in most handling processes, so this is not a surprise. It should be noted that in industrial practice, the thermoset powder is heated up before being spread over the build plate. In selective laser sintering (SLS), the powder is heated just below its melting temperature, causing neighbouring powder particles to join and form neck regions at their area of contact, through atomic diffusion. Such sintering processes are slow, and ill-suited for SLS processes equipped with fast laser-scanning speeds, as such powdered material is usually preheated before it can be sintered.

Furthermore, a lower size and shape segregation was observed in the tested metal powders spread with both recoaters, at both location 1 and 2, compared with the tested plastic powders. This might be due to the lower elongation indexes and size spans of the tested metal powders, compared to the tested plastic powders. The low-level size and shape segregation across the build plate raised the topic of how the tested two-metal powders segregate during transportation. This problem can be further investigated using the QPM rolling segregation tester [30].

In terms of the median particle size, D_{50}: location 2 has a higher value of D_{50} compared to location 1; i.e., on average, larger particles are deposited in location 2, and smaller particles are deposited near deposition point 1. A similar trend was observed by Lee et al. [16]

and Chen et al. [6], wherein the proportion of large particles increased in the direction of the blade recoater during spreading. This could explain why site 2 has a larger relative packing fraction than location 1. This trend has not been seen in the PP2 powder. Location 1 has a higher D_{50} compared to location 2, when spreading PP2 with the recoater IB. Again, this is almost certainly due to the lower flowability of this powder (higher $1/ff_c$), compared to the other tested powders.

Table 2 indicates that the powder's D_{90} at location 2 is slightly higher than, or in the same range as, D_{90} at location 1 for all the tested powders. This could also justify the higher relative packing fraction of the powder bed at location 2, compared to location 1. In the PBF process, a small change in the powder's D_{90} might be a significant phenomenon. This has significant implications for powder recycling during the build process. If fine particles are always placed first, there will be more coarse particles in the collection bin; thus, if the powders are reused, we will receive coarser particles as we continue through the building phases.

More research is needed to better understand the impact of this size segregation on the final component quality, because it is currently uncertain whether it is significant in this respect and, if so, whether efforts should be made to mitigate it, in order to optimise the part quality. For example, it is unclear how the powder bed segregation affects the heat conductivity of the powder, and how this impacts the artefact quality.

6. Conclusions

The spreading of various metal and plastic powders was evaluated using a new tester designed specifically to analyse powder bed spreading during the PBF process [1]. The variables were the recoater shapes (two levels), gap sizes (two levels), and various powders of different materials with different sizes, shapes, and flow functions. The developed rig, and the measuring methods, have proved capable of determining the properties of, and variations in, the powder structure in the bed, in terms of:

1. The relative packing fraction of the powder, and how this varies across the bed.
2. The variation in the size and shape of the particles across the bed.

The concept of "relative packing fraction" has been introduced in this paper, as a way of taking out the differences in bulk density when studying the effect of the spreading operation on the powder. This is defined as the bulk density in the bed, divided by the bulk density reached when the powder is settled via shearing under stress in a shear cell (or tapping in a cylinder, which can give very similar results under the right conditions). The relative packing fraction of the tested powders increased in the direction of the powder spreading; i.e., the powder relative packing fractions were higher in location 2 (near the collection point), compared to location 1 (near the deposition point). The higher relative packing fractions were also observed when spreading powders with the NB recoater, with the higher cross-sectional, radiused edges, and the flat "nose" on the bottom. The higher bed relative packing fraction attained with this recoater is attributed partly to the fact that this recoater design tends to apply a downwards force to the particles as they pass under the rounded edge of the blade. Additionally, this recoater has a flat surface held above the particles for several millimetres of travel after they pass under the leading edge, helping to settle the particles, and prevent them from rotating and "flipping" upwards, which can happen when a sharp edge passes above.

The powder flowability is an important variable affecting the powder bed's relative packing fraction. The relative packing fractions of powders with a lower flowability, i.e., higher $1/ff_c$ (higher cohesiveness), were lower than powders with a better flowability. In this study, the powders with a narrow particle size distribution had higher relative packing fractions, compared to the powders with a wider particle size distribution.

Although the powder build plate was relatively small, at 200 mm square, the size segregation was often quite apparent over the powder bed, as follows.

- A higher fraction of fine and rounded particles is deposited at location 1, while more elongated and large particles are deposited in location 2.

- When utilising an NB recoater, the elongation index is lower than when using an IB recoater, which could explain why the relative packing fraction was lower when using IB recoater than the NB recoater.
- Powders with a higher $1/ffc$ have a lower tendency towards segregation, compared to powders with a lower $1/ffc$. A higher cohesion between particles is well known to lead to a lower segregation tendency in the powder, in most handling processes.

Author Contributions: Conceptualization, H.S.; methodology, H.S., J.C., A.H., T.D. and M.B.; formal analysis, H.S., and M.B.; investigation, H.S. and V.G.; resources, E.G.; writing—original draft preparation, H.S.; writing—review and editing, M.B. and A.H.; supervision, M.B. and A.H.; project administration, J.C.; funding acquisition, M.B. All authors have read and agreed to the published version of the manuscript.

Funding: We thank the EPSRC Future Manufacturing Hub in Manufacture using Advanced Powder Processes (MAPP) for providing the grant for this study.

Data Availability Statement: The data used for this study will be provided upon request.

Conflicts of Interest: The authors declare no conflict of interest.

References

1. Salehi, H.; Cummins, J.; Gallino, E.; Harrison, N.; Hassanpour, A.; Bradley, M. A new approach to quantify powder's bed surface roughness in additive manufacturing. *Powder Technol.* **2022**, *407*, 117614. [CrossRef]
2. Soundararajan, B.; Sofia, D.; Barletta, D.; Poletto, M. Review on modeling techniques for powder bed fusion processes based on physical principles. *Addit. Manuf.* **2021**, *47*, 102336. [CrossRef]
3. Xiang, Z.; Yin, M.; Deng, Z.; Mei, X.; Yin, G. Simulation of Forming Process of Powder Bed for Additive Manufacturing. *J. Manuf. Sci. Eng.* **2016**, *138*, 081002. [CrossRef]
4. Jacob, G.; Brown, C.U.; Donmez, A. *The Influence of Spreading Metal Powders with Different Particle Size Distributions on the Powder Bed Density in Laser-Based Powder Bed Fusion Processes*; NIST Advanced Manufacturing Series; US Department of Commerce, National Institute of Standards and Technology: Gaithersburg, MD, USA, 2018.
5. Mussatto, A.; Groarke, R.; O'neill, A.; Obeidi, M.A.; Delaure, Y.; Brabazon, D. Influences of powder morphology and spreading parameters on the powder bed topography uniformity in powder bed fusion metal additive manufacturing. *Addit. Manuf.* **2020**, *38*, 1101807. [CrossRef]
6. Chen, H.; Chen, Y.; Liu, Y.; Wei, Q.; Shi, Y.; Yan, W. Packing quality of powder layer during counter-rolling-type powder spreading process in additive manufacturing. *Int. J. Mach. Tools Manuf.* **2020**, *153*, 103553. [CrossRef]
7. Muñiz-Lerma, J.A.; Nommeots-Nomm, A.; Waters, K.E.; Brochu, M. A Comprehensive Approach to Powder Feedstock Characterization for Powder Bed Fusion Additive Manufacturing: A Case Study on AlSi7Mg. *Materials* **2018**, *11*, 2386. [CrossRef]
8. Egger, G.; Gygax, P.; Glardon, R.; Karapatis, N. Optimization of powder layer density in selective laser sintering. In Proceedings of the 10th Solid Freeform Fabrication Symposium (SFF), Austin, TX, USA, 9–11 August 1999.
9. Ma, Y.; Evans, T.M.; Philips, N.; Cunningham, N. Numerical simulation of the effect of fine fraction on the flowability of powders in additive manufacturing. *Powder Technol.* **2019**, *360*, 608–621. [CrossRef]
10. Gürtler, F.; Karg, M.; Dobler, M.; Kohl, S.; Tzivilsky, I.; Schmidt, M. Influence of powder distribution on process stability in laser beam melting: Analysis of melt pool dynamics by numerical simulations. In Proceedings of the 25th Annual International Solid Freeform Fabrication Symposium—An Additive Manufacturing Conference, Austin, TX, USA, 4–6 August 2014.
11. Yao, D.; An, X.; Fu, H.; Zhang, H.; Yang, X.; Zou, Q.; Dong, K. Dynamic investigation on the powder spreading during selective laser melting additive manufacturing. *Addit. Manuf.* **2020**, *37*, 101707. [CrossRef]
12. Zhang, J.; Tan, Y.; Bao, T.; Xu, Y.; Xiao, X.; Jiang, S. Discrete Element Simulation of the Effect of Roller-Spreading Parameters on Powder-Bed Density in Additive Manufacturing. *Materials* **2020**, *13*, 2285. [CrossRef]
13. Desai, P.S.; Higgs, C.F. Spreading Process Maps for Powder-Bed Additive Manufacturing Derived from Physics Model-Based Machine Learning. *Metals* **2019**, *9*, 1176. [CrossRef]
14. Yan, W.; Qian, Y.; Ma, W.; Zhou, B.; Shen, Y.; Lin, F. Modeling and Experimental Validation of the Electron Beam Selective Melting Process. *Engineering* **2017**, *3*, 701–707. [CrossRef]
15. Meier, C.; Weissbach, R.; Weinberg, J.; Wall, W.A.; Hart, A.J. Critical influences of particle size and adhesion on the powder layer uniformity in metal additive manufacturing. *J. Mater. Process. Technol.* **2018**, *266*, 484–501. [CrossRef]
16. Lee, Y.; Gurnon, A.K.; Bodner, D.; Simunovic, S. Effect of Particle Spreading Dynamics on Powder Bed Quality in Metal Additive Manufacturing. *Integrating Mater. Manuf. Innov.* **2020**, *9*, 410–422. [CrossRef]
17. Fouda, Y.M.; Bayly, A.E. A DEM study of powder spreading in additive layer manufacturing. *Granul. Matter* **2020**, *22*, 10. [CrossRef]

18. Snow, Z.; Martukanitz, R.; Joshi, S. On the development of powder spreadability metrics and feedstock requirements for powder bed fusion additive manufacturing. *Addit. Manuf.* **2019**, *28*, 78–86. [CrossRef]
19. Haeri, S.; Wang, Y.; Ghita, O.; Sun, J. Discrete element simulation and experimental study of powder spreading process in additive manufacturing. *Powder Technol.* **2017**, *306*, 45–54. [CrossRef]
20. Haeri, S. Optimisation of blade type spreaders for powder bed preparation in Additive Manufacturing using DEM simulations. *Powder Technol.* **2017**, *321*, 94–104. [CrossRef]
21. Han, Q.; Gu, H.; Setchi, R. Discrete element simulation of powder layer thickness in laser additive manufacturing. *Powder Technol.* **2019**, *352*, 91–102. [CrossRef]
22. Nan, W.; Pasha, M.; Bonakdar, T.; Lopez, A.; Zafar, U.; Nadimi, S.; Ghadiri, M. Jamming during particle spreading in additive manufacturing. *Powder Technol.* **2018**, *338*, 253–262. [CrossRef]
23. Berry, R.; Bradley, M.; McGregor, R. Brookfield Powder Flow Tester—Results of Round Robin Tests with Crm-116 limestone powder. *Proc. Inst. Mech. Eng. Part E J. Process. Mech. Eng.* **2014**, *229*, 215–230. [CrossRef]
24. Salehi, H.; Barletta, D.; Poletto, M. A comparison between powder flow property testers. *Particuology* **2017**, *32*, 10–20. [CrossRef]
25. Jenike, A. *Storage and Flow of Solids*; Bulletin No. 123; Engineering Experiment Station, University of Utah: Salt Lake City, UT, USA, 1964.
26. Haydari, Z. The Spreading Behaviour of Stainless Steel Powders for Additive Manufacturing. Master's Thesis, University of Leeds, Leeds, UK, 2021.
27. Wei, L.C.; Ehrlich, L.E.; Powell-Palm, M.J.; Montgomery, C.; Beuth, J.; Malen, J.A. Thermal conductivity of metal powders for powder bed additive manufacturing. *Addit. Manuf.* **2018**, *21*, 201–208. [CrossRef]
28. Sillani, F.; de Gasparo, F.; Schmid, M.; Wegener, K. Influence of packing density and fillers on thermal conductivity of polymer powders for additive manufacturing. *Int. J. Adv. Manuf. Technol.* **2021**, *117*, 2049–2058. [CrossRef]
29. Jacob, G.; Donmez, A.; Slotwinski, J.; Moylan, S. Measurement of powder bed density in powder bed fusion additive manufacturing processes. *Meas. Sci. Technol.* **2016**, *27*, 115601. [CrossRef]
30. Deng, T.; Garg, V.; Salehi, H.; Bradley, M.S. An experimental study on free-surface rolling segregation and correlations with angle of repose and particle sphericity. *Powder Technol.* **2021**, *379*, 307–320. [CrossRef]